Environmental Science and Pollution Research (2024) 31:28321–28340
https://doi.org/10.1007/s11356-024-33082-7

RESEARCH ARTICLE

A hybrid system for Nickel ions removal from synthesized wastewater using adsorption assisted with electrocoagulation

Jean Claude Nizeyimana[1,2,3] · Pamphile Ndagijimana[4] · Junaid Khan[1] · Liu Xiangru[1] · Gratien Twagirayezu[3,5] · Habasi Patrick Manzi[2,3] · Olivier Irumva[6] · Chang-Ping Yu[2] · Anyi Hu[2] · Shanshan Lin[1]

Received: 26 November 2023 / Accepted: 21 March 2024 / Published online: 27 March 2024

Abstract

The presence of heavy metal ions in water environments has raised significant concerns, necessitating practical solutions for their complete removal. In this study, a combination of adsorption and electrocoagulation (ADS + EC) techniques was introduced as an efficient approach for removing high concentrations of nickel ions (Ni^{2+}) from aqueous solutions, employing low-cost sunflower seed shell biochar (SSSB). The combined techniques demonstrated superior removal efficiency compared to individual methods. The synthesized SSSB was characterized using SEM, FT-IR, XRD, N_2-adsorption–desorption isotherms, XPS, and TEM. Batch processes were optimized by investigating pH, adsorbent dosage, initial nickel concentration, electrode effects, and current density. An aluminum (Al) electrode electrocoagulated particles and removed residual Ni^{2+} after adsorption. Kinetic and isotherm models examined Ni^{2+} adsorption and electrocoagulation coupling with SSSB-based adsorbent. The results indicated that the kinetic data fit well with a pseudo-second-order model, while the experimental equilibrium adsorption data conformed to a Langmuir isotherm under optimized conditions. The maximum adsorption capacity of the activated sunflower seed shell was determined to be 44.247 $mg.g^{-1}$. The highest nickel ion removal efficiency of 99.98% was observed at initial pH values of 6.0 for ADS and 4.0 for ADS/EC; initial Ni^{2+} concentrations of 30.0 mg/L and 1.5 g/L of SSSB; initial current densities of 0.59 mA/cm^2 and 1.32 kWh/m^3 were also found to be optimal. The mechanisms involved in the removal of Ni^{2+} from wastewater were also examined in this research. These findings suggest that the adsorption-assisted electrocoagulation technique has a remarkable capacity for the cost-effective removal of heavy metals from various wastewater sources.

Keywords Heavy metals · Coupled adsorption + electrocoagulation · Biochar · Environmental remediation

Introduction

The increasing levels of heavy metal ions in aquatic ecosystems pose a serious threat to human health due to their persistent nature and detrimental impacts (Jaishankar et al. 2014). According to Di Natale et al., nickel and other heavy metal ions are found in many different types of water, including those from wastewater treatment plants, industrial effluents, and aquatic environments. The presence of nickel ions in water reservoirs is a cause for serious worry, necessitating targeted attention and measures to reduce the negative effects of heavy metal pollution (Di Natale et al. 2020). The possible effects of nickel contamination on human and environmental health make it an issue that requires deep investigation. Different industrial processes, such as metal coating, metal cleaning, battery production, electronics, electroplating, fertilizer smelting, car emissions, and uncontrolled fertilizer use, release nickel ions into water systems (Šuránek et al. 2021) (Jiang et al. 2019). Moreover, nickel ions have the potential to enter the human body through the food chain, where they accumulate in various tissues and organs. This accumulation poses health risks and threatens vital systems, as highlighted in studies such as (Khan et al. 2013). An increased risk of kidney illness, cardiovascular problems, lung cancer, dermatitis, and other health concerns in humans has been connected to prolonged exposure to nickel through food intake and water consumption (Liakos et al. 2021). Given these concerns, it is critical to protect public health by creating effective methods for removing nickel ions from water. Nickel removal from

Responsible Editor: Weiming Zhang

Extended author information available on the last page of the article

wastewater is an issue that has been addressed by numerous technologies in recent years. These technologies encompass various approaches such as reverse osmosis (Ali 2018), ion exchange (Yan et al. 2020), plasma and electrochemistry coupling (Spanos et al. 2017), membrane separation (Zhang et al. 2019), adsorption (Kumari et al. 2020), electrodialysis (Sano et al. 2018), electrocoagulation (Ii et al. 2020), and chemical precipitation (Tanong et al. 2017). These advancements have shown promising results. However, some limitations have been identified, including the need for large amounts of chemicals, high operational and capital costs, production of secondary sludge, and sensitivity to operating conditions.

Adsorption (ADS) has emerged as a prominent technology for removing nickel ions, attracting considerable attention due to its effectiveness and cost efficiency. Various adsorbent materials have been extensively investigated for their nickel removal capabilities. These materials encompass a diverse range, such as polymer resins, zeolites, biochar, biological materials, chitin, activated carbon, eggshells, sunflower shells, clays, and mineral oxides. The exploration of these adsorbents reflects the ongoing efforts to identify versatile and efficient materials for nickel removal from wastewater(Burakov et al. 2018).

Biochar-based adsorbents have particularly attracted interest due to their cost-effectiveness and high adsorption efficiency. In this study, sunflower seed shell biochar (SSSB) was chosen as a special adsorbent due to its availability and low cost. However, it is important to note that biochar alone may exhibit relatively low removal efficiency and an inability to degrade pollutants completely, leaving residual pollutants in the water solution. Therefore, there is a need to enhance the adsorption capacity of biochar for its potential future applications. Electrocoagulation (EC) is another powerful electrochemical process that involves the continuous in-situ generation of a coagulant from polluted water. EC can destabilize, polarize, and dissociate suspended particles in wastewater under a uniform electric field (Heidmann and Calmano 2008). By utilizing EC, the efficiency of removing pollutants from water can be improved. Overall, the combination of adsorption and electrocoagulation techniques holds promise for the efficient removal of nickel ions from wastewater. It provides a cost-effective and environmentally friendly approach to address the challenges associated with nickel contamination.

In this study, aluminum electrodes were employed as both the anode and the cathode (Al-Al configuration). By utilizing a DC power supply to apply current to the fluid medium, the electrocoagulation (EC) process was initiated, resulting in the formation of coagulants. This process involves the dissolution of aluminum ions from the aluminum electrodes. At the anode, metal ions are generated through electrolytic oxidation, while water molecules undergo simultaneous hydrolysis. Simultaneously, hydrogen gas is produced at the cathode. The formation of hydrogen bubbles causes pollutants to rise to the surface of the solution, facilitating their concentration, collection, and easier removal compared to when they are dispersed throughout the solution (Huang et al. 2020). The overall reactions occurring in the EC process can be summarized in three successive steps, as depicted by the equations below (Channa et al. 2019). Firstly, at the anode, the sacrificial aluminum anode undergoes a dissolution reaction, generating aluminum ions:

$$Al_{(s)} \rightarrow Al^{3+}_{(aq)} + 3e^- \quad (1)$$

The cathode also acts as a site for the electrolysis of water, where a reduction reaction takes place in the bulk solution. Through electrolysis, hydrogen gas is formed at the surface of the cathode. The generated gas bubbles facilitate flotation during the reduction reaction. Consequently, the nickel ions form agglomerates, which gather into larger clusters and float to the water's surface, making their removal easier.

$$2H_2O + 2e^- \rightarrow H_{2(g)} + 2OH^- \quad (2)$$

$$2H_2O \rightarrow 4H^+ + O_{2(g)} + 4e^- \quad (3)$$

(ii) The outcomes of the EC process include the destabilization of pollutants, suspension of particulate matter, and breakup of emulsions. Additionally, as the pH of the wastewater increases, hydroxide ions are generated at the cathode. This leads to the precipitation of nickel ions, as well as their hydroxides, and co-precipitation with aluminum hydroxides.

$$Ni^{2+} + 2OH^- \rightarrow Ni(OH)_{2(g)} \quad (4)$$

(iii) The last stage involved the stabilization of the coagulation phases, leading to the formation of flocs. Furthermore, the anodic nickel ions and hydroxide ions produced at the electrode surfaces react with the contaminated water, resulting in the generation of different aluminum hydroxides within the electrocoagulation system.

$$Al^{3+}_{(aq)} + 3OH^- \rightarrow Al(OH)_{3(s)} \quad (5)$$

Although using electrocoagulation (EC) technology alone may not be cost-effective and sometimes results in the generation of additional pollutants, combining EC with adsorption can offer advantages such as cost reduction, recovery and recycling of pollutants in water solutions, and complete elimination of contaminants. Our study aims to achieve two objectives: (1) treating highly contaminated wastewater using a small amount of sunflower seed shell biochar (SSSB) to minimize time and energy consumption compared to using either adsorption (ADS) or EC alone, and (2) preparing SSSB from sunflower seed shells without

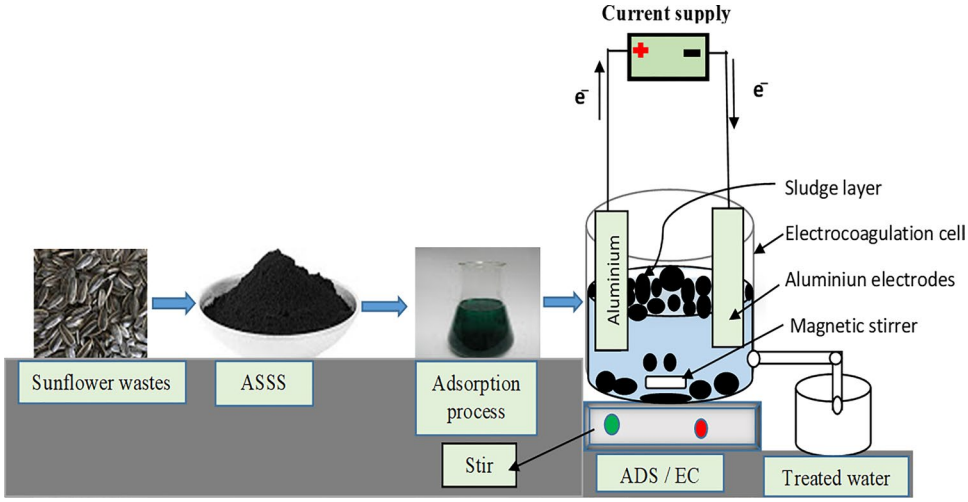

Fig. 1 Schematic representation of experimental set-up

any modification and characterizing its properties using techniques such as scanning electron microscopy (SEM), Fourier-transform infrared spectroscopy (FT-IR), X-ray photoelectron spectroscopy (XPS), Brunauer–Emmett–Teller (BET) analysis, X-ray diffraction (XRD) and Transmission Electron Microscopy (TEM).

To accomplish these goals, adsorption using non-modified SSSB combined with electrocoagulation at a low current density and minimal cost were selected. The operating parameters, including the adsorbent dosage, pH, initial nickel concentration, different electrode materials, and current density, were optimized. Our study also calculated the total operating cost of Ni^{2+} removal in the EC cell. Additionally, adsorption isotherm and kinetic studies were conducted to understand the adsorption mechanisms.

The findings of this study provide valuable insights and information for effectively removing highly concentrated heavy metals from wastewater.

Materials and methods

Materials preparation

The Sunflower Seed Shell (SSS) was obtained from a local market and underwent a thorough washing process using both tap water and distilled water to remove surface pollutants. Afterward, it was dried for 30 min to eliminate moisture content before being crushed into a powder using a crushing machine. The resulting powder was sieved to obtain particles with a size of 0.45 µm. Subsequently, the SSS powder was heated at 500 °C for 2 h under a nitrogen gas environment using a muffler to produce the sunflower seed shell-based biochar (SSSB) adsorbent. After a cooling period of 5 h, the prepared samples were washed with ultrapure water and dried at 105 °C for 7 h. The final products were stored in polyethylene bags for further experiments and characterization. No additional modifications or chemical reagents were used before the adsorption experiments.

Preparation and characterization of chemical agents

Analytical-grade chemicals, including nickel chloride hexahydrate ($NiCl_2{\cdot}6H_2O$) (purity > 98.0%, molecular weight of 237.69 g/mol, Sodium hydroxide (NaOH), (purity > 96.0% molecular weight is 40 g/mol, sodium chloride (NaCl) (purity > 98.0%, molecular weight of 58.44 g/mol, and hydrochloric acid (HCl, purity 36.5%, molecular weight of 36.46 g/mol) and all chemicals are supplied by Sino-pharm Chemical Reagent Co., Ltd. Stock solutions of Ni^{2+} with a concentration of 1000 mg/L were prepared using nickel $NiCl_2{\cdot}6H_2O$ to create synthetic wastewater. A solution of 0.1 M NaOH and HCl was utilized for initial pH adjustments. Aluminum (Al-Al) plates [(99.5% purity), 30 cm × 20 m × 0.05 cm] were employed as the anode and cathode electrodes, which were purchased from Taobao Inc.

Adsorption experiments

Figure 1 illustrates the experimental setup for the adsorption studies. The experiments were conducted in 250 mL Erlenmeyer flasks containing 100 mL of solution with an initial concentration of 30 mg/L of nickel metal ions. Different dosages of SSSB ranging from 0.1 to 3 g were added to the flasks. The experiments were carried out at room temperature, and the initial pH of the solution was varied between 2 and 8. To ensure proper mixing, an orbital shaker was employed to agitate the flasks for 2 h at a constant room temperature of 25 °C and a shaking speed of 150 rpm. After the completion of the agitation process, the materials were filtered using a 0.45 µm filter paper (Whatman) and analyzed using a flame atomic

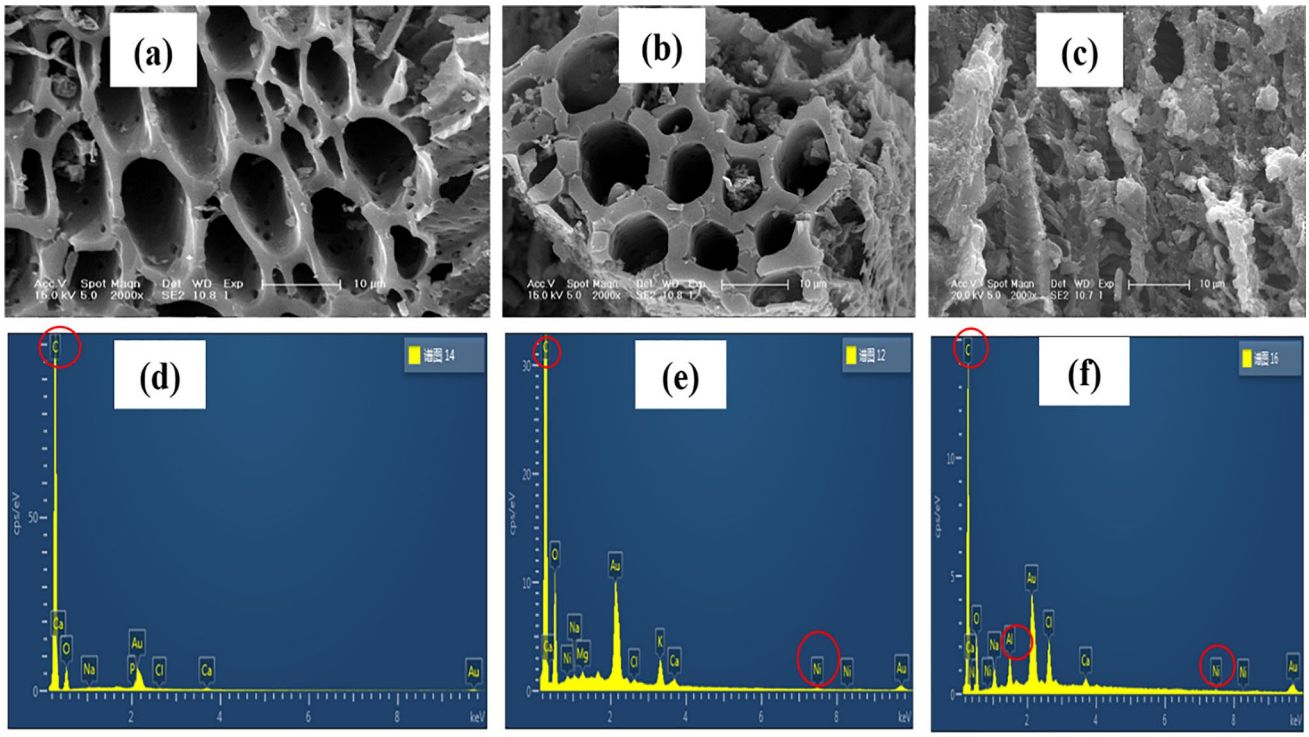

Fig. 2 **a** illustrates the surface morphology analyzed by SEM before ADS, **b** SEM after ADS, and (**c**) SEM after ADS + EC while (**b**) EDS before ADS, **e** EDS after ADS, and (**f**) EDS after ADS + EC images

absorption spectrophotometer (AAS Z-5000, Japan). The removal efficiencies (R) of Ni^{2+} were calculated using Eq. 6.

Electrocoagulation experiments

The experimental setup, as depicted in Fig. 1, involved the construction of a Plexiglas electrocoagulation cell with dimensions of 14 cm × 10 cm × 14 cm. Each experiment utilized approximately 650 mL of synthetic wastewater. The sacrificial electrodes were aluminum (Al) plates measuring 12 cm in height, 7 cm in width, and 0.2 cm in thickness. These electrodes were arranged in a monopolar configuration, with a spacing of approximately 10 mm between them. To maintain a constant current, a precision DC power supply (GW GPC-3060D) with current and voltage ranges of 0–6 A and 0–30 V, respectively, was utilized. Sodium chloride (NaCl) was added to the wastewater to increase its conductivity and achieve different values. The pH of the wastewater was measured using an Inola WTW pH meter and adjusted using a 0.1 M NaOH solution. During the electrocoagulation (EC) process, the effluent from the adsorption (ADS) step was agitated at 150 rpm using a magnetic stirrer. Before use, the electrodes were cleaned with 0.1 M HCl, a brush, and distilled water to remove rust and contaminants, followed by drying in an oven for 10 min. Samples of 10 mL were taken from the electrocoagulation cell every 5 min for analysis, while the cell was maintained at 6.0 V. The sludge was filtered using a Whatman 0.45 µm filter, and the nickel ion content was evaluated using a flame-atomic absorption spectrophotometer. The removal efficiency of nickel ions was calculated using Eq. 6.

$$\%R = \frac{(C_0 - C_e)}{C_0} 100 \tag{6}$$

The amount of nickel ions absorbed can be calculated using the following Eq. (7).

$$q_e = \frac{V}{m}(C_0 - C_e) \tag{7}$$

where C_0 and C_e are the initial and final concentration of Ni^{2+} mg L^{-1}, m is the amount of SSSB (g) and V is the volume of solution (mL.L^{-1}).

Characterization of adsorbent

The mineral composition and surface morphology of the activated sunflower seed shell (SSSB) were analyzed using scanning electron microscopy (SEM) and energy dispersive X-ray spectroscopy (EDS) analysis. The SEM analysis was performed using a JEM-2100F microscope operating at 200 kV. The functional groups responsible for the adsorption of nickel ions on the SSSB surface were determined using Magna 560

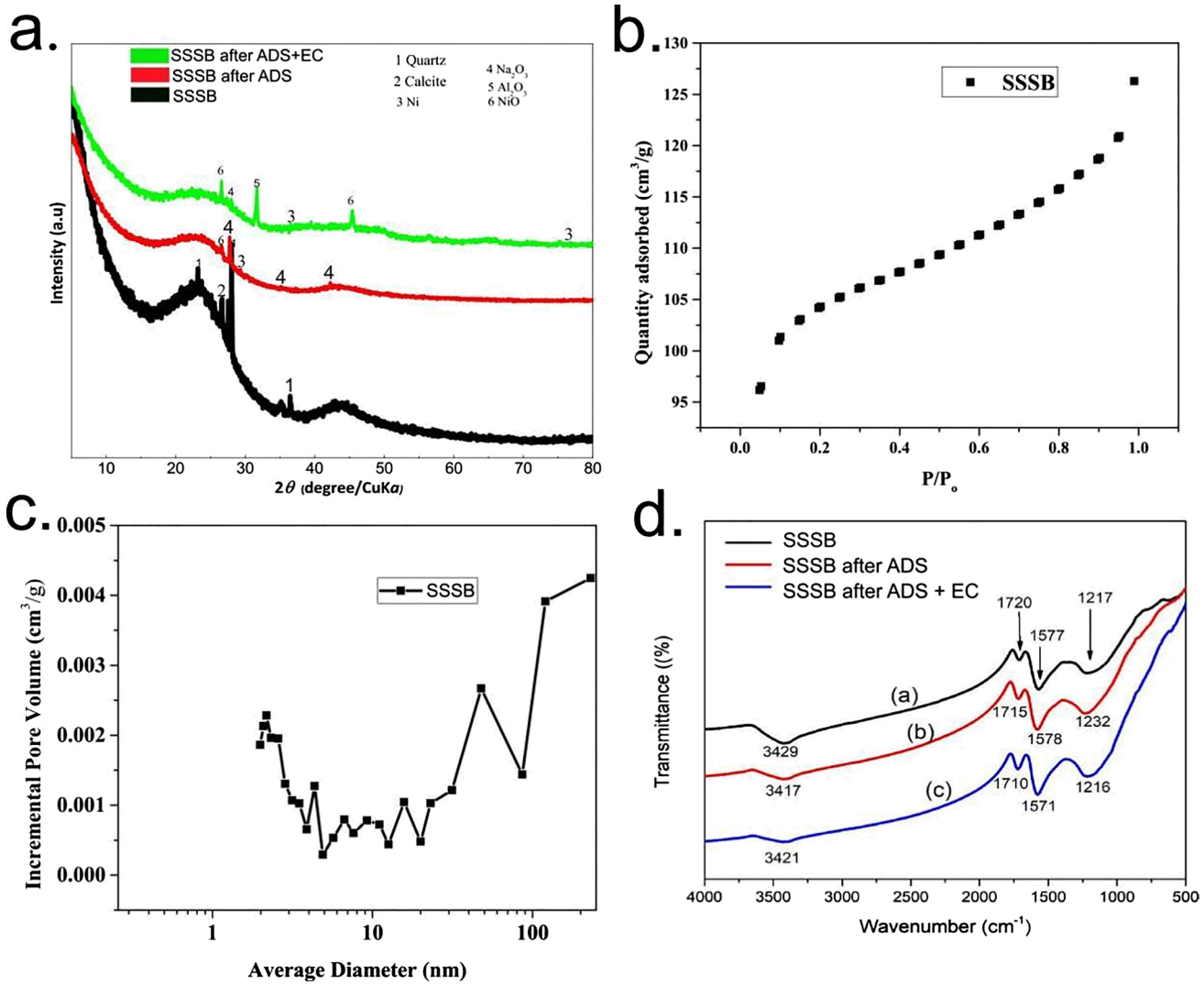

Fig. 3 **a** XRD characterization, **b** N2 adsorption–desorption, **c** porous distribution, and (**d**) FT-IR spectroscopy characterization

Fourier-transform infrared spectroscopy (FTIR). The crystallographic behavior of the SSSB before and after adsorption was evaluated using X-ray diffraction (XRD) with a Rigaku D/MAXYA diffractometer equipped with a Ni-filtered Cu source. The specific surface area of the SSSB and the pore size distribution were determined using the Brunauer–Emmett–Teller (BET) method and a volumetric adsorption system (Micromeritics ASAP 2020 MC) at 77 K. The chemical composition and elemental valence of the SSSB-based adsorbents were analyzed using X-ray photoelectron spectroscopy (XPS) with a Thermo Scientific Escalab 250Xi instrument.

Energy consumption and amount of dissolved electrodes

The energy consumption in the electrocoagulation treatment process plays a crucial role in its financial implications. It is directly related to the applied electric current and voltage in the treatment system. To determine the energy required for the removal of Ni^{2+} from the solution, the following equation was employed:

$$\mathrm{EC}\left(\mathrm{kWh.m^{-3}}\right) = \frac{\mathrm{I \times t \times v}}{1000\mathrm{V}} \tag{8}$$

where EC energy consumption in kilowatt-hours per cubic meter ($\mathrm{kWh.m^{-3}}$), I represents the electric current in amperes (A), v is the applied voltage in volts (V), t is the reaction time in hours (h), and V is the volume of the sample in cubic meters (m^3). Furthermore, Faraday's law describes the mass of aluminum electrodes dissolved in the solution and is expressed as:

$$m_{Al} = \frac{I \times t \times M_w}{ZF} \tag{9}$$

Table 1 Textural structure of SSSB materials in this study

Adsorbent	S_{BET} ($m^2\ g^{-1}$)	Pore volume ($cm^{-3}\ g^{-1}$)	Pore size (nm)
SSSB	331.74	0.171	2.00

where m_{Al} is the mass of dissolved aluminum electrode (kg/m^3), I the current (A), t is the electrolysis time (s), M_w is the molecular mass of Al (26.98 g/g.mol), z is the number of electrons involved in the reaction Al (3) and Faraday's constant (96,485.34 C/mol).

Result and Discussion

Characteristic of adsorbent

Figure 2a depicts the surface morphology of the SSSB before its application, revealing an angular and uniform pore structure with significant porosity and a pristine composition without any deposited compounds within the pores. On the other hand, Fig. 2b shows visible rough flaws in the agglomerated surface morphology, along with a pore structure that facilitates the effective deposition of nickel ions after the adsorption process. The influence of nickel ions on the SSSB surface after exposure to ADS + EC is evident in Fig. 2c, with clean and irregular cracks as well as cylindrical shapes indicating the absorption of nickel ions and contaminants containing aluminum hydroxides (Jain et al. 2020). Figure 2d demonstrates that the pyrolyzed biomass has a high carbon content, which contributes to the adsorption of pollutants from wastewater due to the presence of carbon-based functional groups (Elabbas et al. 2020). The appearance of a new intensity peak in Fig. 2e indicates the successful adsorption of nickel ions from the solution onto the SSSB sample after the introduction of the $NiCl_2.6H_2O$ compound, highlighting the efficient performance of our adsorbent material during the ADS process. In Fig. 2f, the dissolution of aluminum from the electrodes and the widespread presence of nickel ions across the SSSB surface are observed during the ADS + EC process. The enhanced nickel adsorption is attributed to the active sites depicted in Fig. 2c, thus confirming the synergistic mechanism of ADS and ADS + EC in the removal of higher concentrations of Ni^{2+} when combined.

Figure 3a displays the crystal behavior of biochar before and after adsorption. The pristine amorphous biochar exhibited diffraction peaks in the range of 20° to 40°, corresponding to crystalline graphite-like structures such as quartz (SiO_2) and calcite, respectively. The intensity of these peaks decreased after ADS and ADS + EC treatments (Hubetska et al. 2021). Additionally, new peaks emerged at 30° and 45° on the adsorbents following both treatments, with ADS + EC showing a greater number of new peaks.

Figure 3b presents the image of porous distribution, revealing the presence of micro-mesopores and macropores, which are crucial for effective Ni^{2+} adsorption. The textural behavior of the SSSB is depicted in Fig. 3c, obtained by evaluating the N_2 adsorption–desorption isotherm curves. The isotherms correspond to type IV according to the IUPAC classification, indicating the presence of micro-mesopores in the pristine biochar. The hysteresis loops within the P/P0 range of 0.1–1.0 further confirm the existence of micro-mesopores.

Table 1 demonstrates that the prepared biochar exhibits a relatively good specific surface area (SBET = 331.74 $m^2\ g^{-1}$), which is advantageous for the adsorption process. Figure 3d and Table 2 display the FTIR spectra of the SSSB before adsorption (raw material), after ADS, and ADS + EC, along with the main aspects of these spectra and their respective assignments, as documented by Mohamed et al. (Mohamed et al. 2017).

The following assignments can be made based on these spectra: An intense and broadband in the wavenumber range of 3500–3100 cm^{-1}, indicating the presence of primary and secondary amines and amides. Peaks at 3429, 3417, and 3421 cm^{-1} are attributed to the stretching of H-bonded alcohols, phenols, primary and secondary amines, amides, and carboxylic acids (O–H and N–H). Similar results were observed by (Baysal et al. 2018). New peaks were detected at 1720, 1715, and 1710 cm^{-1}, which can be attributed to aldehydes, ketones, and carboxylic acids

Table 2 Summary of peak location for every functional group analyzed in FT-IR spectra for raw and Ni^{2+} loaded activated sunflower seed shell

Types of bond	Functional groups	Wavenumber (cm^{-1})		
		Before ADS (Raw)	After ADS	After ADS + EC
O–H N–H	alcohols, phenols, primary, secondary amines, and amides stretch, and carboxylic acid	3429	3417	3421
C = O	Aldehyde, ketone, and carboxylic acid	1720	1715	1710
N–H	Primary, secondary amines and amides bend	1577	1578	1571
C–O C–N	Alcohol, ethers, carboxylic acids and anhydrides, and amines	1217	1232	1216

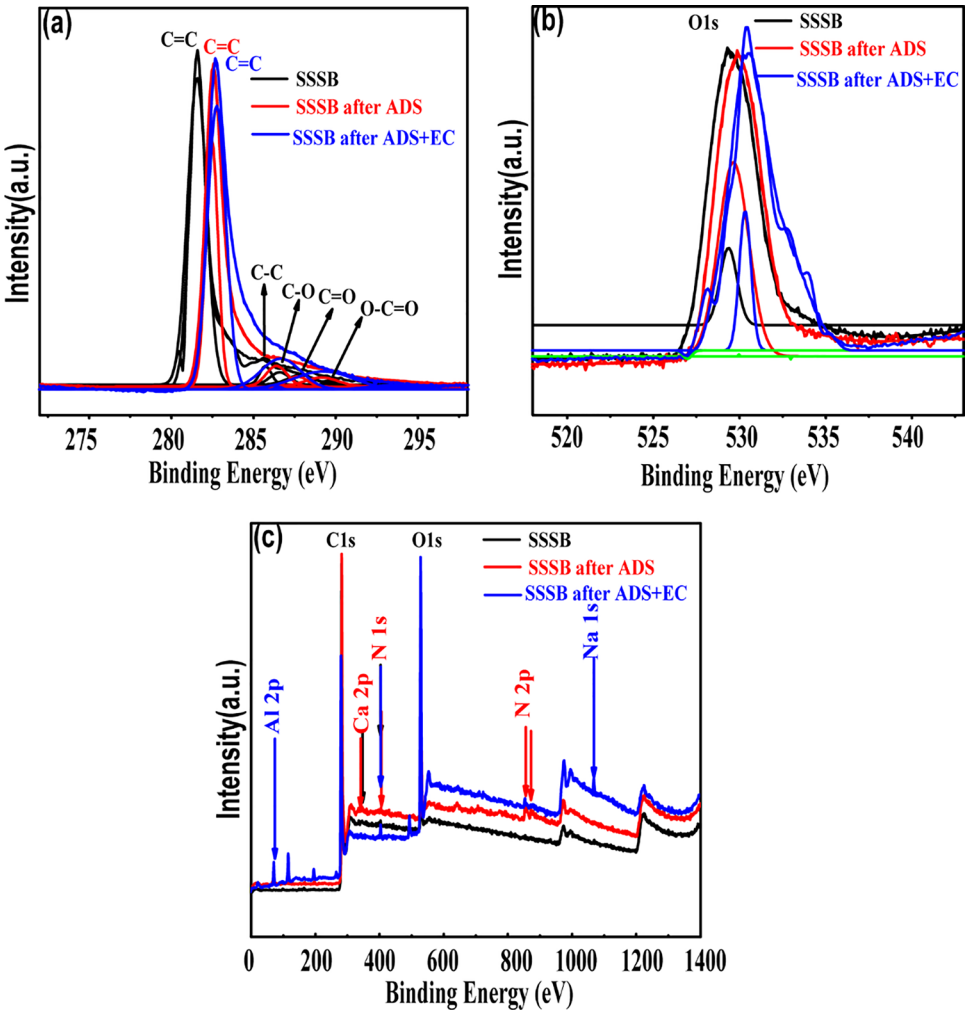

Fig. 4 XPS characterization of sunflower seed shell biochar (SSSB)

(C = O) (Mohamed et al. 2017; Abdulhussein and Al wared 2019). Peaks observed at 1577, 1578, and 1571 cm^{-1}, are indicative of bending vibrations of primary and secondary amines and amides (N–H) (Eletta et al. 2019). Strong peaks were observed at 1217, 1232, and 1216 cm^{-1}, assigned to functional groups such as C–O and C–N, predominantly linked to alcohols, ethers, carboxylic acids, anhydrides, and amines (Jain et al. 2015). Hence, the presence of carboxylic acids, amines, alcohols, and ethers groups in SSSB plays a significant role in adsorbing nickel ions from wastewater. Additionally, the better removal of Ni^{2+} is observed when adsorption is coupled with electrocoagulation. These results indicate that SSSB effectively eliminates Ni^{2+} through its textural properties (microporosity and surface area) as well as its heterogeneous functional groups.

XPS surveys were conducted on the prepared SSSB before adsorption (Fig. 4a), after ADS (Fig. 4b), and after ADS + EC (Fig. 4c). In Fig. 4a-c, the wide scan analysis of SSSB before and after adsorption is described. Notably, new peaks corresponding to oxygen (O1s), carbon (C1s), and nitrogen (N1s) were observed between 275 and 600 eV on the SSSB before and after ADS, as well as after ADS + EC. These peaks signify the presence of carbon–oxygen functional groups, which are advantageous for the adsorption of targeted pollutants, particularly Ni2 +, onto the surface of the SSSB adsorbent. A slight increase in the nitrogen (N1s) band from 399.3 to 399.5 eV indicates the formation of complexes between SSSB and Ni^{2+}. This suggests that a pair of ion electrons from nitrogen atoms are shared with nickel ions, resulting in a decrease in electron cloud density around the nitrogen atoms and giving rise to a higher band energy peak (Yuan et al. 2022). The changes observed in the carbon (C1s) and oxygen (O1s) peaks after ADS and ADS + EC, as shown in Fig. 4, demonstrate the involvement of carbon–oxygen functional groups in the adsorption process. Furthermore, new peaks corresponding to aluminum (Al), calcium (Ca), sodium (Na), and nickel (Ni) were detected on the surface of the used adsorbents after ADS and ADS + EC, as depicted in Fig. 4c. The presence of the two peaks at 856.8 and 872.7 eV in the nickel (Ni 2p) spectrum confirms the presence of nickel on the surface of the SSSB after ADS and ADS + EC.

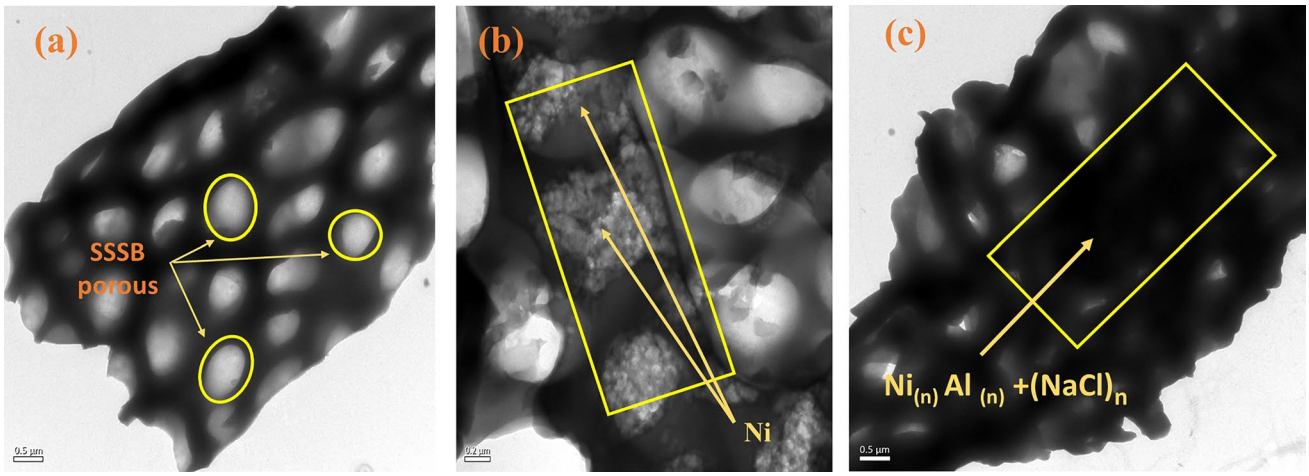

Fig. 5 Transmission electron microscopy analyzed by TEM before ADS, (**b**) TEM after ADS, and (**c**) TEM after ADS + EC

Figure 5 shows the results of a transmission electron microscopy (TEM) study that compared the surface properties of SSSB materials used before ADS, after ADS, and with ADS + EC. The results reveal that a porous network shape of SSSB can be seen in the SSSB-TEM micrograph depicted in Fig. 5a. Here, the presence of Ni(0) ions on the absorbent is indicated by the white spots. In both Fig. 5b and c, which represent SSSB materials subjected to TEM after

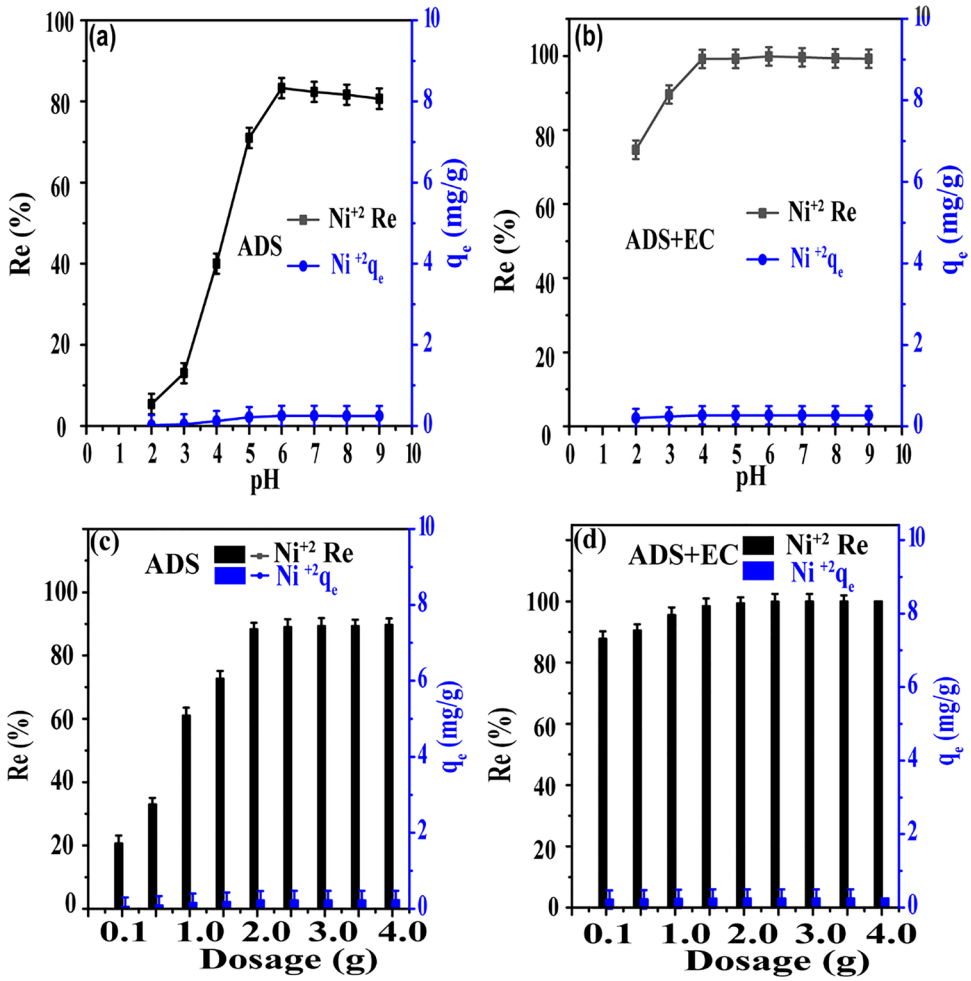

Fig. 6 **a**, **b** effect of pH for ADS and ADS + EC, and (**c**, **d**) effect of dosage for ADS and ADS + EC

Table 3 Isotherm parameters for Ni^{2+} ADS/EC coupling process

Langmuir model		Freundlich model		Temkin		D-R model	
Parameters	Ni	Parameters	Ni	Parameters	Ni	Parameters	Ni
K_L(L/mg)	0.03688	K_f (mg/g)(L/mg)$^{1/n}$	0.2888	A	9.00568	q_m(mg/g)	5.283
q_m(mg/g)	44.247	n	1.7615	B	1.35973	β (mol^2/k^2/j^2	7.37E-08
R^2	0.984	R^2	0.958	R^2	0.95847	E(kj/mol)	2604.262
						R^2	0.83246

ADS and ADS + EC, respectively, the materials exhibit fine agglomerations of Nickel ions with dense and disordered pores. However, Fig. 5c reveals a higher presence of contaminants filling the pores compared to Fig. 5b. This indicates that a greater amount of Ni ions has been adsorbed during ADS + EC. This observation aligns with findings reported by Prakash and Seyed Hossein (Om Prakash et al. 2020; Mousavi et al. 2023).

Effect of parameters

Effect of pH

When combining ADS with EC techniques, such as SSSB adsorption and an Al electrode, the pH of the aqueous solutions plays a crucial role and exerts a significant influence. The experimental results illustrating the effects of varying the initial solution's pH on both processes are presented in Fig. 6a and 6b. Extensive research has demonstrated that the pH of ADS can affect the ability of biosorbents to remove pollutants (Jiang et al. 2009; Patil et al. 2019). For ADS (Fig. 6a), the removal efficiency increased within the pH range of 6.0 and slightly decreased at pH 8.0, with a notable removal efficiency of 81.03% for Ni adsorption from SSSB. In acidic conditions, the binding of nickel ions to SSSB was hindered due to surface charges and the presence of functional groups. This can be attributed to the competition between hydrogen ions and Ni^{2+} on the surface of SSSB. The -OH and -COOH functional groups on the SSSB adsorbent play a significant role in targeted adsorption (Abdulhussein and Al Wared 2019). Therefore, these functional groups undergo Ni^{2+} ion exchange and dissociate across a range of pH values. The negatively charged surfaces of the adsorbent facilitate the adsorption of nickel ions. In the case of the ADS + EC process for Ni^{2+} removal, the optimal pH value was found to be 4.0, as depicted in Fig. 6b. As the pH increased from 2.0 to 4.0, the Ni^{2+} removal efficiency increased from 81.03% to 99.96%. Notably, at pH 4.0, the highest removal percentage of 99.98% was achieved. However, when the solution's pH exceeded 7.0, there was a slight decrease in Ni^{2+} removal. The pH plays a crucial role in chemical coagulation as it governs the presence of various metal hydroxides in the system. In the pH range of 2.0–4.0, $Al(OH)_2^+$ and Al^{3+} are the predominant metal species involved in chemical coagulation. Conversely, at alkaline pH, $Al(OH)_4^-$ may become the dominant ion species despite its weaker floc-forming ability (Balouchi et al. 2020). Equations (10) and (11) suggest that in highly alkaline solutions, the system's performance may be compromised as OH ions attack the

Table 5 Kinetic parameters for Ni^{2+} ADS/EC coupling process: HRT, 20 min; initial pH, 6.0; Adsorbent dose, 1.5 g/L and current density = 0.59 mA/cm^2 in the presence of Al-Al electrode

Models	Parameters	Ni ions in the system
Pseudo-first-order	K_1(1/min)	0.00115
	q_e (mg/g)	4.206
	R^2	0.905
Pseudo-second-order	K_2 (g/mg.min)	0.0590
	q_e (mg/g)	19.030
	R^2	0.974
Intraparticle diffusion	K_{dif}	3.27772
	C	5.73486
	R^2	0.66923

Table 4 Comparison of the maximum capacities of nickel ions in other studies that used sunflower adsorbents

Sunflower adsorbents	q_m(mg/g)	References
Sunflower (Tithonia diversifolia) stalk	35.84	(Abdulhussein and Al wared 2019)
Sunflower pith	965 and 580	(Baysal et al. 2018)
Sunflower Seed Husks	79.37	(Sahu et al. 2014)
Sunflower seed husks	18.56	(Jean Claude et al. 2022)
sunflower stem (Helianthus annuus)	4.9 and 3.6	(Jain et al. 2016)
sunflower seed shell	44.247	This study

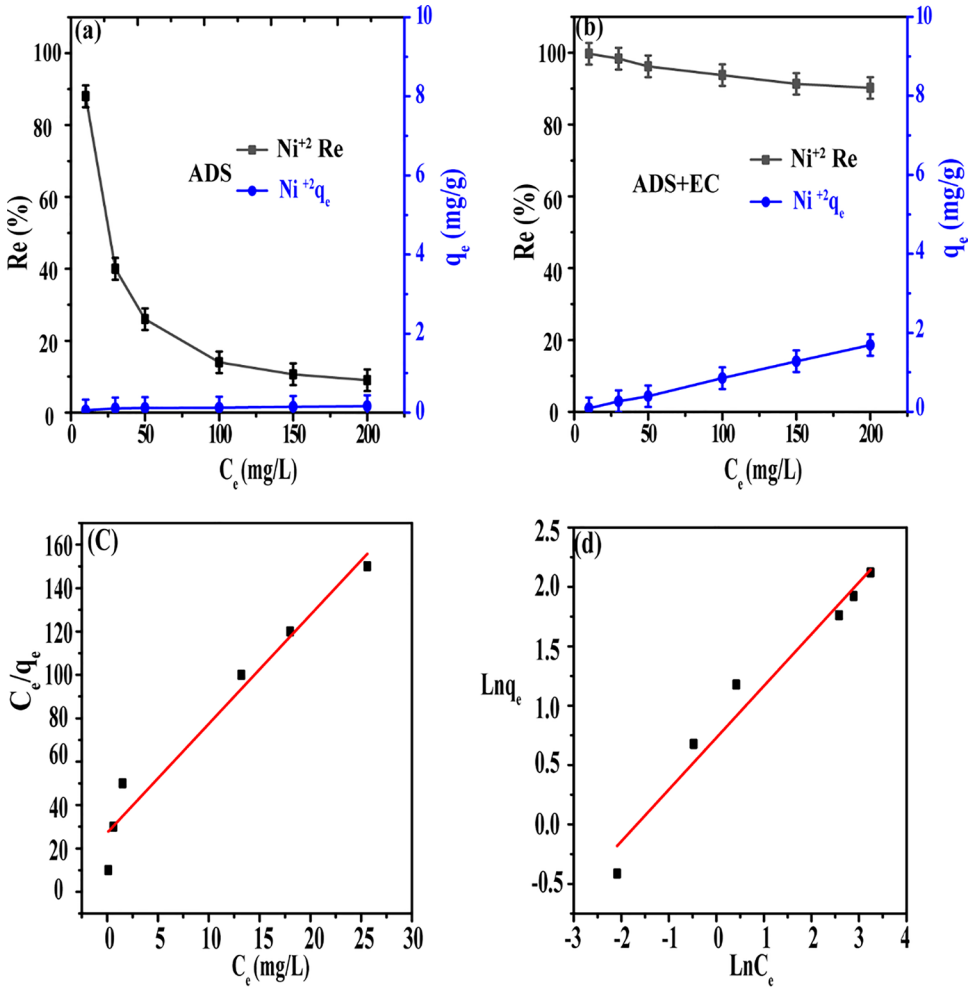

Fig. 7 **a**, **b** effect of initial concentration for ADS and ADS + EC, and (**c**, **d**) Langmuir and Freundlich isotherm fitting model

cathode electrode, resulting in the formation of $Al(OH)_4^+$ instead of $Al(OH)_3^+$(Bazrafshan et al. 2015).

$$2Al_{(s)} + 6H_2O + 2OH^- \rightarrow 2Al(OH)_4^- + 3H_2 \quad (10)$$

$$Al(OH)_3 + OH^- \rightarrow 2Al(OH)_4^- \quad (11)$$

In Figure S1, the distribution of aluminum hydrolysis species based on pH has been shown. Various hydroxylated cation forms are produced by reacting Al^{3+} and OH^- with different medium pH values. Up until pH 3.5, the free cation Al^{3+} is the most abundant ion in acidic environments. The distribution of several hydroxo-complexes, including monomers and polymers, changes as the pH rises. These complexes include $Al(OH)^{2+}$, $Al(OH)_2^+$, $Al_2(OH)_2^{4+}$, $Al(OH)_4^-$, and polymeric species such as $Al_6OH_{15}^{3+}$, $Al_7OH_{17}^{4+}$, etc. In the pH range of 4 to 9, aluminates can be found in the solid phase, which is formed by precipitating the neutral form of $Al(OH)_3$ and its polymerized structures (Reaction (12) (Lekhlif et al. 2014).

$$nAl(OH)_3 \rightarrow Al_n(OH)_{3n} \quad (12)$$

Effect of adsorbent dosage

The effect of dosage was investigated for both ADS and ADS + EC, as depicted in Figures 5c and 6d. The dosage range of 0.1–3.0 g/L was utilized while keeping the values of other operating parameters such as time, pH, and initial concentration constant. Within the ADS process (Fig. 6c); a substantial removal efficiency (Re) of 88.0% was achieved with an adsorbent dosage of 0.5 to 1.5 g/L. At equilibrium, when the adsorption process was completed, the solution was transferred to the Electrocoagulation cell and subjected to treatment at a current density of 0.59 mA/cm^2. The results demonstrate that the ADS + EC process significantly enhances the Ni^{2+} removal rate compared to the ADS technique alone (Fig. 6c and 6d). In under 20 min, the Ni^{2+} removal efficiency was elevated to 98.98% from 88.0% in the ADS + EC process, representing a substantial increase of 10.98% (Fig. 6d). These findings highlight that increasing the dosage of SSSB enhances the effectiveness of Ni^{2+} removal. Interestingly, within the ADS + EC method, a remarkable efficiency of 99.9% was achieved using a low SSSB dosage of 0.5 g/L. Therefore, it is evident that

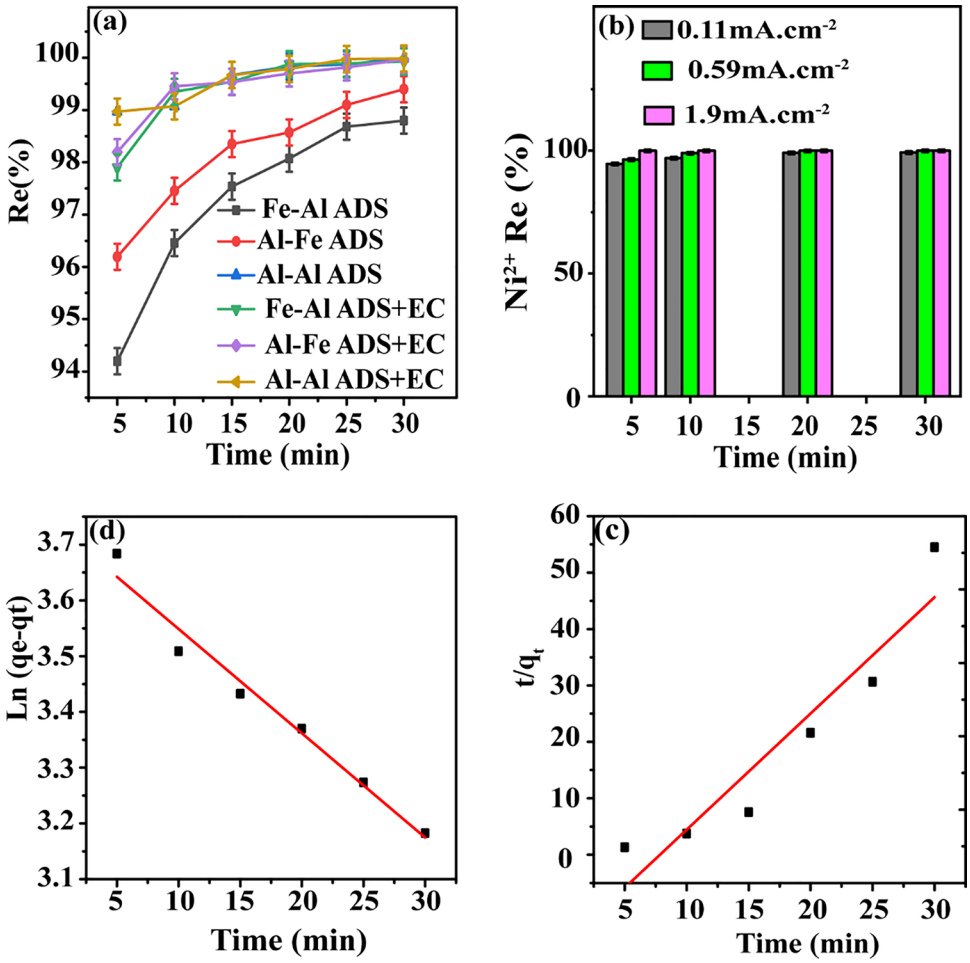

Fig. 8 **a** effect of different types of electrodes, **b** effect of current density, **c** PFO fitting kinetic model, and (**d**) PSO fitting model kinetics

at low adsorbent dosages, the combined ADS + EC technique exhibits great potential for enhancing the efficiency of metal ion removal from wastewater, as demonstrated by Vasudevan (Vasudevan et al. 2011). However, increasing the adsorbent dosage does not impact Ni^{2+} adsorption due to the saturation of active sites on the adsorbent (Rathour et al. 2016; Sikdar et al. 2020).

Effect of initial concentration

In the investigation of the effect of initial concentration, an SSSB dosage of 0.5 g/L and varying Ni^{2+} concentrations of 10, 30, 50, 100, 150, and 200 mg/L were employed. Figure 7a and 7b illustrate the impact of initial concentration on Ni^{2+} removal efficiencies, where Re increased at lower initial concentrations, while qe (mg/g) increased with higher initial concentrations. For the ADS process, the removal efficiencies of SSSB for Ni^{2+} adsorption were 88.4%, 40.6%, 26.4%, 14.6%, 10.7%, and 9.0%, respectively (Figure 6a). In the ADS + EC process, the removal efficiencies ranged from 99.7% to 99.3%, 96.2% to 91.3%, and 90% to 22% as the initial concentration increased, as depicted in Fig. 7b. The increase in Re for ADS at lower concentrations can be attributed to the rapid bonding of Ni^{2+} ions to available adsorption sites (Abdulhussein and Al wared 2019). In contrast, in the ADS + EC process, the slower coagulation at higher initial concentrations led to a decrease in removal efficiency. The amount of coagulants ($Al(OH)_3$) generated in ADS + EC remained relatively constant, which can result in electrode passivation and affect the efficiency of metal removal from the solution. However, it should be noted that the initial Ni^{2+} concentration values could not be eliminated by this volume of sludge. Similar findings have been reported by Farihahusnah Hussin, where initial Ni^{2+} concentrations above 50 mg/L showed limited reduction during the ADS + EC process due to slower coagulation rates, which resulted in lower removal efficiency. Additionally, Zakaria has described comparable findings (Salem and Majeed 2019).

Effect of electrodes

Using a fixed potential difference of 7 V, a current of 50 mA, a Ni^{2+} concentration of 30 mg/L, and a contact time of 20 min, the ADS + EC method was employed

to investigate the influence of Al- and Fe-based electrode materials on Ni^{2+} removal from aqueous solutions. Experiments were conducted in a reactor using different electrode combinations (Fe–Fe, Al-Al, Al–Fe, and Fe-Al) under the same operational conditions to assess the system's effectiveness in Ni^{2+} removal. The hydraulic retention time for Ni^{2+} removal was examined, and the results (Fig. 8a) showed maximum metal removal of 96.9%, 99.87%, 99.70%, and 99.78% with the Fe–Fe, Al-Al, Al–Fe, and Fe-Al electrode combinations, respectively, after 20 min. These findings indicated a higher rate of Ni^{2+} removal during the first 10 min of operation, followed by a decrease, possibly due to inadequate coagulant dosage. This discrepancy in removal efficiency could be attributed to the varying release rates of ions from the Al and Fe electrodes. The Al electrodes released more ions into the solution compared to the Fe electrodes, resulting in higher sludge production. Considering that the Al electrodes exhibited higher efficiency than the Fe electrodes, it is logical to prioritize further research involving Al electrodes. Bhagawan et al., supporting our findings (Bhagawan et al. 2014), reported similar results.

Effect of current density

The adsorption coupled with the electrocoagulation process can be influenced by the current density, as it affects factors such as coagulant dosage, bubble formation, and the size and growth of flocs. Higher current densities lead to increased anode dissolution and the formation of metal hydroxide flocs in greater quantities, resulting in improved pollutant removal. In this study, three different current densities, namely 0.11, 0.59, and 1.19 mA/cm^2, were employed to assess their effects on Ni^{2+} removal, as depicted in Fig. 8b. The results of the coupled adsorption with electrocoagulation revealed that the nickel removal efficiency increased with higher current densities. After 20 min, removal yields of 99.01%, 99.93%, and 99.98% were achieved at current densities of 0.11, 0.59, and 1.19 mA/cm^2, respectively. Notably, the highest removal efficiency was attained at a current density of 0.59 mA/cm^2, which is relatively low compared to the findings of the Elabbas study. This suggests that the electric current utilized in this study is sufficiently low, accomplishing the main objective of reducing operating expenses. In this scenario, the increase in situ production of Al $(OH)_3$ leads to the flocs acting as an adsorbent for the nickel ions. The high removal efficiency can be attributed, in part, to the co-precipitation of Ni (II) ions with aluminum hydroxides resulting from an elevated pH. Similar results have been reported (Balouchi et al. 2020).

Adsorption modeling

Adsorption Isotherm modeling

In this study, the adsorption isotherm model was used to examine the interaction between the adsorbate and adsorbents at a specific temperature. The four models that are used frequently in this study are the Langmuir and Freundlich, (Khan et al. 2021), Temkin (Matouq et al. 2015), and Dubinin – Radushkevich (D-R) Isotherm models (Chen et al. 2022) were utilized. The higher coefficients (R^2), as shown in Table 3, typically indicate a better fitting quality. Further information on the Temkin and D-R isotherm models can be found in the supporting information (Text S1). The Langmuir model assumes that adsorption occurs on a homogeneous surface through monolayer coverage without any subsequent interaction among the adsorbed species. The equation for the Langmuir model is as follows:

$$\frac{1}{q_e} = \frac{1}{q_m K_L C_e} + \frac{1}{q_m} \tag{13}$$

Here, q_e is the equilibrium adsorption capacity of Ni^{2+} metal ions onto SSSB (mg/g), qm is the maximum monolayer coverage capacity (mg/g), K_L is the Langmuir isothermal constant (L/mg), and Ce is the equilibrium adsorbate concentration (mg/L). The Langmuir plot (Fig. 6c) shows the relationship between $1/q_e$ and 1/Ce, and its slope and intercept can be used to calculate q_m and K_L. An important parameter of the Langmuir isotherm model is the equilibrium parameter R_L, which is a dimensionless constant indicating the adsorption nature as shown in Table 3. It can be calculated as:

$$R_L = \frac{1}{1 + K_L C_O} \tag{14}$$

Here, Co represents the initial concentration of the metal ion (mg/L), and K_L refers to the Langmuir isotherm constant. The value of R_L provides insights into the adsorption behavior, such as unfavorable adsorption ($R_L > 1$), linear adsorption ($R_L = 1$), favorable adsorption ($0 < R_L < 1$), and irreversible adsorption ($R_L = 0$), (Yargiç et al. 2015).

The Freundlich isotherm is an empirical model that describes multilayer adsorption on a heterogeneous surface of the adsorbent. It can be used to explain adsorption equilibrium using Eq. 14.

$$lnq_e = \frac{1}{n} lnC_e + lnK_F \tag{15}$$

K_F stands for the Freundlich isotherm constant (in milligrams per gram of adsorbent), q_e stands for the quantity of metal adsorbed per gram of adsorbent at equilibrium (in milligrams per gram), Ce stands for the adsorbate concentration

Table 6 Comparison between the results of this study and previous studies

Topic	Coupled techniques	Maximum removal (%)	Optimum parameters	EEC (KWh/m^3)	Reference
An experimental study of sunflower seed husk and zeolite as adsorbents of Ni(II) ion from industrial wastewater	N/A	76	pH 6.5, 20 g/L of adsorbent, time = 2 h	N/A	(Tadayon et al. 2023)
Nickel removal from wastewater using an electrocoagulation process with zinc electrodes under various operating conditions: performance investigation, mechanism exploration, and cost analysis	N/A	99.4	The current density = 10 mA/cm^2, pH = 9.2, and the gap distance 4 cm and time = 90 min	23.79	(Shaker et al. 2021)
Removal of low concentrations of nickel ions in electroplating wastewater by a combination of electrodialysis and electrodeposition	electrodialysis and electrodeposition	92	Cell voltage: 1.6–3.2 V, Flow rate: 10–90 mL min^{-1}, Electrolysis time: 1–9 h, Electrolyte, pH: 3–7, and Ni(II) concentration: 0.2–2 mg L^{-1}	2.4	(Kong et al. 2019)
Electrooxidation of nickel-ammonia complexes and simultaneous electrodeposition recovery of nickel from practical	Electrooxidation and electrodeposition	99	Current density: 32 mA/cm^2; electrolyte pH: 9; Ni(II) concentration: 2.16 g L^{-1} and deposition time: 3 h	0.11	(Guan et al. 2017)
Treatment of CNC industry wastewater by electrocoagulation technology: an application through response surface methodology	N/A	89.94	pH 10; time = 30 min; Ni(II) concentration = 4.11 mg/L; Cost = 8.50 €/m^3 for aluminum electrode	N/A	(Oden 2020)
Removal of nickel ion from electroplating wastewater using double chamber electrodeposition cell (DCEC) reactor partitioned with water hyacinth (*Eichhornia crassipes*) leaves	Double chamber electrodeposition cell and single chamber electrodeposition cell (SCEC)100 (DCEC)59 (SCEC)	100 (DCEC) 59 (SCEC)	Potential: 5 V, Ni(II) concentration: 2.2 g L^{-1} and Deposition time: 72 h	30	(Kane et al. 2016)
A hybrid system for Nickel ions removal from synthesized wastewater using adsorption assisted with electrocoagulation	Adsorption and electrocoagulation	99.98	pH 4.0–6.0, initial Ni^{2+} concentration of 30 mg/L, SSSB dosage of 1.5 g, and current density: 0.59 mA/cm^2	1.32	This work

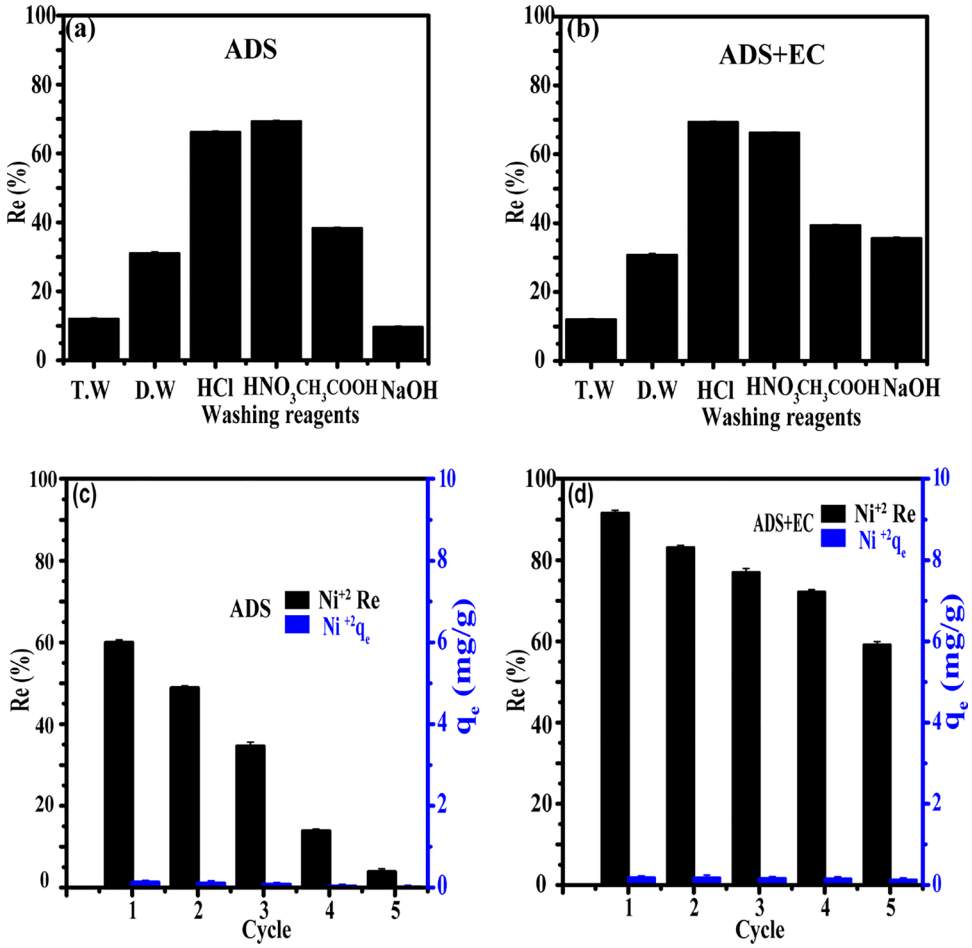

Fig. 9 **a**, **b** Effect of washing of adsorbents after ADS and ADS + EC, and (**c**, **d**) Recycling of SSSB after ADS and ADS + EC

at equilibrium (in milligrams per liter), and 1/n stands for the adsorption density. The values of K_F and n are determined from the slope and intercept of the graph of $\log(q_e)$ versus log(Ce), as shown in Fig. 7d. The calculated values of K_F and n are presented in Table 5. The value of n provides information about the adsorption behavior. If n is greater than 1 ($n > 1$), the adsorption is favorable, while if n is lower than 1 ($n < 1$), the adsorption is considered poor (Taylor et al. n.d.). The data obtained from the Langmuir and Freundlich models are presented in Table 3. As shown in Table 3 and Fig. 7c, d, the isotherm parameters for nickel ions in the ADS + EC coupling process with a hydraulic retention time of 20 min, initial pH of 6.0, and adsorbent dose of 1.5 mg/L in the presence of Al-Al electrode were calculated. The results indicate that the Langmuir isotherm model provided a better fit with a higher regression coefficient $R^2 = 0.984$ compared to the Freundlich isotherm $R^2 = 0.958$. This suggests that nickel ions are adsorbed by SSSB and form a monolayer on its surface, as indicated by the higher regression coefficient.

Based on the Langmuir isotherm model, the maximum adsorption capacity (q_m) was calculated as 44.247 mg/g at 25 °C. A comparison of this maximum adsorption capacity with other SSSB materials from previous studies is presented in Table 4. The higher regression coefficient indicates the formation of a monolayer of nickel ions on the surface of the SSSB adsorbent, with specific active sites on a homogeneous surface being involved in Langmuir adsorption. Using Eq. 13, the R_L value was determined to be greater than 0 and less than 1 ($R_L = 0.47$) when the initial concentration of Ni^{2+} was 30 mg/L, and 1.5 g of SSSB was used, with an agitation speed of 150 rpm and a working temperature of 30 °C. This suggests that the adsorption of Ni^{2+} ions on SSSB is favorable. In summary, the Freundlich isotherm model can be expressed as follows:

$$lnq_e = \frac{1}{n} lnC_e + lnK_F \tag{16}$$

The Temkin and D-R models are described in detail in Text S1. The R^2 values in Table 3 clearly show that these models did not provide a better fit than the Langmuir model.

Adsorption Kinetic modeling

Adsorption kinetics involves analyzing the rate of solute uptake and the time required for absorbing a substance. In this study, the concentration of Nickel ions at time q_t (mg/g)

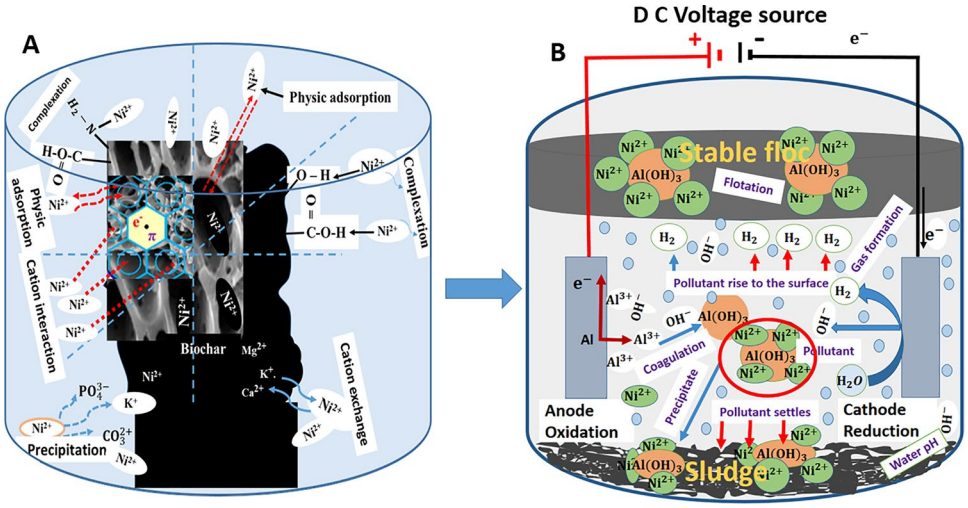

Fig. 10 Adsorption-electrocoagulation mechanism

was investigated. Before applying the adsorbent material in further applications, it is important to understand its kinetic parameters and adsorption characteristics. Contact time, temperature, and the initial Ni^{2+} concentration are three key factors to consider in the adsorption process (Jiang et al. 2009). Three kinetic models, namely the Pseudo-first-order (PFO), pseudo-second-order (PSO), and intraparticle diffusion models, were utilized to analyze Ni^{2+} adsorption on sunflower seed shell-based biochar and aluminum electrodes. These models can be expressed as follows:

$$\ln\left(q_e - q_t\right) = lnq_e - K_1 t \tag{17}$$

$$\frac{1}{q_t} = \frac{1}{K_2 q_e^2} + \frac{t}{q_t} \tag{18}$$

$$q_t = K_d t^{0.5} + C \tag{19}$$

Here, q_t represents the amount of adsorbed metal ions per gram of adsorbent at any given time (mg/g), q_e is the number of metal ions adsorbed per gram of adsorbent at equilibrium (mg/g), K1 is the adsorption rate constant (min^{-1}), K_2 is the adsorption rate constant (g/mg/min), $K_2\ q_e^2$ represents the initial adsorption speed, t is a constant time (min) and k_d (mg/[$gmin^{0.5}$]), intraparticle diffusion rate constant. The adsorption rate constant K_1 is calculated from the slope of the graph plotted for $\ln(q_e—q_t)$ against t, and the theoretical q_e value is determined from the breakpoint on the graph (Fig. 8c, d). Similarly, the adsorption rate constant K_2 and theoretical q_e values are calculated from the slope and breakpoint of the graph plotted for t/q_t against t (Fig. 8d). The data for kinetics fitting parameters are presented in Table 5 and Fig. 8(c and d). The results indicate that the pseudo-second-order (PSO) model provides a better fit to the experimental data than the pseudo-first-order (PFO) model, as evidenced by the correlation coefficient $R^2 = 0.974$ and $R^2 = 0.905$, respectively, in Table 5. The calculated q_e value from the PSO model shows a very good agreement with the experimental value (Table 5). The pseudo-second-order kinetic model is expressed in Eq. 17. The determination of the diffusion process, specifically the rate-determining step of the adsorption process, was conducted using intraparticle diffusion (Eq. 18) (Mousavi et al. 2023). The R^2 values in Table 5 indicate that the intraparticle diffusion did not control the adsorption process.

Desorption and reusability experiments

For effective adsorbents to be considered of high quality and efficiency, they must possess certain fundamental characteristics such as reusability and the ability to undergo the desorption process effectively. Desorbing metals from used adsorbent is crucial to continue utilizing the spent adsorbent, recover valuable compounds, and reduce operating costs in wastewater treatment. Some studies have shown that complete reversibility of metal ion adsorption on certain adsorbents is not achievable (Abdulhussein and Al wared 2019). To desorb adsorbed Ni^{2+} ions from aqueous solutions, six different desorbing agents were employed: HCl, HNO_3, CH_3OOH, NaOH, distilled water (D.W), and treated water (T.W). The desorption efficiency varied among these solutions, with 0.1 M HCl exhibiting the highest recovery rate for Ni^{2+}, followed by HNO_3, CH_3OOH, NaOH, D.W, and T.W in descending order. As illustrated in Fig. 9a and b, 0.1 M HCl achieved a maximum desorption of 93.3% for Ni^{2+}, while HNO_3, CH_3OOH, NaOH, D.W, and T.W desorbed approximately 87.4%, 61.7%, 58.4%, 52.2%, and 36.0% of the adsorbed nickel ions, respectively. Similar findings were reported by Mohammed et al., (Mohammed 2015), who observed that the highest desorption of Ni^{2+} occurred with HCl concentrations ranging from 0.025 M to 0.175 M. Among the desorbing agents, HCl was utilized for the chemical regeneration of the spent SSSB and Al-electrode after ADS + EC

processes for Ni^{2+} removal from synthetic wastewater. It was successfully chemically reused and recycled up to five times. As depicted in Fig. 8c and d, the regenerated adsorbent exhibited relatively good performance, with the removal efficiency decreasing from 91.6% to 59.9%. This decrease in removal efficiency could be attributed to the blockage of pores by adsorbed nickel ions or the repeated digestion of the tiny aluminum electrodes due to acid desorption. Additionally, there might have been a loss of SSSB during the application process. However, despite these factors, the produced adsorbent and electrodes hold the potential for promising future applications in removing nickel ions from wastewater.

Adsorption-electrocoagulation mechanism

The adsorption mechanisms involved in the interaction between SSSB, nickel, pH of the solution, and other conditions can be explained by their physicochemical properties. The presence of pores on SSSB, as observed in SEM and BET results, plays a key role in the adsorption of Ni^{2+}. Additionally, the functional groups present on the surface of SSSB, as indicated by FTIR and XPS analysis, contribute to the adsorption of Ni^{2+} on SSSB's surface. Figure 10a illustrates that the adsorption mechanisms of nickel by SSSB involve factors such as pore structure, surface area, hydrogen bonding, pi-pi interactions, electrostatic interactions, precipitation, and complexation. The mechanisms involved in the adsorption coupled with electrocoagulation (ADS + EC), as depicted in Fig. 10b, were evaluated. The electrocoagulation method utilizes an electrochemical process with a sacrificial anode, often made of aluminum (Al). The EC system comprises both physical and chemical processes. When an Al anode is used, the following reaction occurs:

$$A1(s) \rightarrow A1^{3+} + 3e^{-}$$

The Al^{3+} ions produced undergo hydrolysis, forming species with high surface areas capable of trapping pollutants through electrostatic attraction or surface complexation. These species include $Al(OH)_4$, $Al(OH)_2{}^{+}$, $Al(H_2O)_6{}^{3+}$, $Al(H_2O)_5\ (OH)_2{}^{+}$, $Al_6(OH)_{15}{}^{3+}$, $Al_7(OH)_{17}{}^{3+}$, $Al_8(OH)_{20}{}^{4+}$, $Al_{13}(OH)_{34}{}^{4+}$, and Al(OH). At the cathode, hydrogen gas and hydroxide ions are produced through the following reaction:

$$2H_2O + 2e^{-} \rightarrow 2HO^{-} + H_2(g)$$

In the presence of chloride anions, Cl can be oxidized to Cl_2, a powerful oxidizer that can enhance the oxidation of dissolved organic molecules or generate ClOH, which also possesses oxidizing properties (Hakizimana et al. 2017):

$$2Cl^{-} \rightarrow Cl_2 + 2e-$$

$$Cl_2 + H_2O \rightarrow ClOH + Cl^{-} + H^{+}$$

Various equilibrium reactions, including acid–base, precipitation, complexation, and redox reactions, occur in the solution at the anode. The EC technique combines the advantages of chemical coagulation, electrochemical, and flotation processes (Ika Pratiwi et al. 2021). The dominant mechanism in an EC system depends on the type of pollutants and the involved processes, which can include: First, electrochemical reduction and oxidation; anode and cathode surfaces undergo electrochemical reduction and oxidation, respectively, following the principles of electrochemistry (Sahu et al. 2014). Secondly, adsorption and charge neutralization; metal cations formed at the anode result in the compression of the electric double layer and a decrease in repulsive forces. Positively charged particles are attracted to the negatively charged metal hydroxide, leading to adsorption and charge neutralization. Sweep coagulation; formation of insoluble metal hydroxide flocs occurs in the solution, acting as traps for precipitation and entrapping pollutants, thereby promoting agglomeration. Coagulants and flocculants can polymerize and generate bridges between particles through the interparticle bridging mechanism. Thirdly, direct adsorption; certain contaminants may be directly attracted to the electrodes through electric forces. The predominating mechanism depends on the substance being removed and the collaborative action of these different mechanisms during the EC process. Figure 10 provides a visual representation of these mechanisms, highlighting the interplay among various processes to effectively remove pollutants, with the predominating mechanism varying depending on the specific pollutant involved (Sahu et al. 2014).

Energy consumption

Energy consumption is a crucial economic parameter in combined treatment processes, and we calculated the energy consumption and mass of dissolved aluminum electrodes using Eqs. (8) and (9) based on our previous research (Jean Claude et al. 2022). Compared to the simple EC process, the incorporation of SSSB leads to a reduction in energy consumption. In the simple EC process, energy consumption is directly proportional to the initial pH value of the solution. However, in the ADS + EC process, the addition of SSSB raises the wastewater's pH value until it reaches 4.0, resulting in decreased energy consumption. After 20 min of wastewater treatment, the ADS + EC process achieved a nickel ion removal efficiency of 99.94%, with an energy consumption of 1.32 kWh/m^3 and a mass of dissolved aluminum electrodes of 1.5×10^{-6} kg/m^3. These results indicate that the ADS + EC process offers a cost-effective treatment method with lower energy consumption. From an economic standpoint, the coupled process is preferable as it requires less time and achieves higher nickel ion removal efficiency compared to single processes (ADS or EC). Furthermore, the coupling technique is more environmentally friendly. The efficiency

of the coupling process in terms of Ni^{2+} removal is inversely proportional to the reduction in energy consumption. In other words, higher Ni^{2+} removal efficiency corresponds to lower energy consumption per m^3 of nickel ions removed from the wastewater. In this study, the ADS + EC coupling method exhibited an energy consumption of 1.32 kWh/m^3, which is lower than the values reported by Ayub and Wagle, (Ayub et al. 2020; Wagle et al. 2020) for EC alone (2.27 kWh/m^3 and 6.9 kWh/m^3, respectively). These findings align with the results of Vasudevan et al. (Vasudevan et al. 2011), who concluded that the combination of ADS and EC processes is highly effective for wastewater treatment, achieving high removal efficiency while consuming minimal energy.

Treatment cost (OC)

The treatment cost was calculated using a formula from our previous study. In this study, the total operating cost for all treatment processes (OC_{Total}) = (Energy consumption × Electricity cost) + (Electrodes consumption × Anode price) + chemical added × Chemicals price (the cost of the hydrochloric acid (HCl) or Sodium Hydroxide (NaOH) needed for pH adjustment) + cost of the treatment for the produced sludge or the summation of the operating cost (OC) and the operating cost of activated carbon (OC_{AC}). The formula for total operating cost is summarized based on our previous study (Jean Claude et al. 2022).

$$OC_{Total}\left[\frac{USD}{m^3}\right] = \left[\frac{(I \times v \times t)C_{kwh} + C_{pH} + \left[\frac{M_{Al} \times I \times t}{z \times F}\right] \times C_{Al} + C_s}{V}\right] + \left[\frac{M_{AC} \times C_{AC}}{V}\right] \quad (20)$$

In this context, where $C_{kWh} = 0.104$ USD kWh^{-1}, $C_{Al} = 454 \times 10^{-8}$ USDKg^{-1}, Cs = 0.083 USD ton^{-1} or m^3, V = 0.0001 m^3, z = 3, Faraday's constant (F) = 96,485.34 C mol^{-1}, the molecular mass of Al (Mw) = 26.98 g g^{-1} mol, I = 0.04956A, v = 6.0 V, t = 20 min, CpH ≈ 0, M_{AC} = 0.5 g and C_{AC} = 0.0981 USD kg^{-1}.

According to Eqs. (10), the calculated operating cost (OC) is found to be 0.0933 USD m^{-3}, including electricity price and transportation distance (max. 40 km), while the operating cost of activated carbon (OC_{AC}) = 0.049 USD Kg^{-1}, respectively. Finally, the total cost (OC_{Total}) of the adsorption combined with the electrocoagulation (ADS + EC) process is approximately 0.142 USD m^{-3}, which is lower than the costs found in other current studies (Lu et al. 2008; Shaker et al. 2023). Notably, the total operation cost depends on the prices of consumables in the market, the costs of sludge management, and the amount of water treatment technologies. Therefore, the wastewater treatment in this study (ADS + EC) adheres to Chinese standard costs.

The comparison with previous studies

We conducted a comparison of our study with previous research works that employed different coupled techniques for nickel ion removal from wastewater. This comparison was made due to the limited availability of studies discussing nickel removal through the combination of adsorption and electrocoagulation in the presence of a sunflower shell as an adsorbent. Therefore, Table 6 shows the results of a comparison between this study and others. After more than 2 h, the removal efficiencies reach their highest level. Reducing the processing time for Ni removal results in lower energy consumption and cost because the removal and the electric energy consumption exceed 99% and 1.32 kWh/m^3 after 20 min, respectively, which can be considered sufficient. In comparison to the previous studies whose findings can be compared to this one, the expense or treatment cost of this study has been reduced (Table 6).

Conclusion

This study focuses on the removal of Ni^{2+} from synthetic wastewater using a combined treatment system of adsorption coupled with electrocoagulation. For the first time, a biochar-based adsorbent derived from sunflower seed shell (SSSB) and the aluminum electrode was employed in this process. The combined approach proved to be cost-effective, exhibiting high removal efficiency while consuming low energy. The results indicated that the highest nickel ion removal efficiency (99.98%) was achieved under optimal conditions, which included an initial pH of 6.0 for adsorption (ADS) and 4.0 for ADS/EC, an initial Ni^{2+} concentration of 30.0 mg/L, SSSB dosage of 1.5 g/L, the current density of 0.59 mA/cm^2, the energy consumption of 1.32 kWh/m^3 and the total treatment cost of 0.142 USD m^{-3}. The combination of adsorption and electrocoagulation techniques offered a more attractive alternative compared to using ADS or EC alone due to its higher nickel removal efficiency. The experimental data fitting revealed that the kinetic data aligned well with a pseudo-second-order model (R^2 = 0.974), while the equilibrium adsorption data followed a Langmuir isotherm (R^2 = 0.984). The maximum adsorption capacity of SSSB was determined to be 44.247 mg/g, and the main adsorption mechanisms involved electrostatic

interactions, precipitation, H-bonding, complexation, and the texture of SSSB. The regeneration of SSSB exhibited promising potential for future applications in Ni^{2+} removal from water. The information gathered from this study holds significant value in the design and investigation of full-scale adsorbent for the treatment of nickel-containing industrial wastewater.

Supplementary Information The online version contains supplementary material available at https://doi.org/10.1007/s11356-024-33082-7.

Acknowledgements This work was supported by the "National Natural Science Foundation of China and Science and Technology Department of Changchun City" Program, the State Key Laboratory of Environmental Geochemistry, and the Northeast Normal University.

CAS Key Laboratory of Urban Pollutant Conversion of Urban Environment, Institute of Urban Environment, Chinese Academy of Sciences.

We also acknowledge the ANSO Scholarship for Young Talents in China from the Chinese Academy of Sciences.

Authors' contributions Altogether authors contributed to the study's conception and design.

Conceptualization and writing—original draft preparation: [Jean Claude Nizeyimana].

Supervision and Resources: [Prof. Shanshan Lin, Prof. Chang-Ping Yu, and Prof. Anyi Hu].

Formal analysis and investigation: [Junaid Khan, Gratien Twagirayezu and Olivier Irumva].

Writing—review and editing: [Shanshan Lin] and [Pamphile Ndagijimana].

Data collection: [Jean Claude Nizeyimana], [Junaid Khan], [Liu Xiangru] and [Habasi Patrick Manzi]. All authors read and approved the final manuscript.

Funding This research paper was financed by the "National Natural Science Foundation of China (NSFC: 41772236) and the Science" and "Technology Department of Changchun City (17SS027)".

Data availability Not applicable.

Declarations

Ethical approval and consent to participate Not applicable.

Consent for publication Not applicable.

Competing interest The authors declare that they have no known competing financial interests or personal relationships that could have appeared to influence the work reported in this paper.

References

Abdulhussein SA, Alwared AI (2019) Single and Binary Adsorption of Cu(II) and Ni(II) Ions from Aqueous Solutions by Sunflower Seed Husk. Assoc Arab Univ J Eng Sci 26:35–43. https://doi.org/10.33261/jaaru.2019.26.1.005

Ali S (2018) Biofillers from Renewable Lignocellulosic feedstock For Elastomers. Scuola Di Dottorato Università Degli Studi Di Milano-Bicocca

Ayub S, Siddique AA, Khursheed MS et al (2020) Removal of heavy metals (Cr, Cu and Zn) from electroplating wastewater by electrocoagulation and adsorption processes. Desalin Water Treat 179:263–271. https://doi.org/10.5004/dwt.2020.25010

Balouchi H, Baziar M, Dehghan A et al (2020) Combination of electrocoagulation and MOF adsorption systems for EBT removal from water. Int J Environ Anal Chem 00:1–11. https://doi.org/10.1080/03067319.2020.1737035

Baysal M, Bilge K, Yılmaz B et al (2018) Preparation of high surface area activated carbon from waste-biomass of sunflower piths: Kinetics and equilibrium studies on the dye removal. J Environ Chem Eng 6:1702–1713. https://doi.org/10.1016/j.jece.2018.02.020

Bazrafshan E, Mohammadi L, Ansari-Moghaddam A, Mahvi AH (2015) Heavy metals removal from aqueous environments by electrocoagulation process - A systematic review. J Environ Health Sci Eng 13. https://doi.org/10.1186/s40201-015-0233-8

Bhagawan D, Poodari S, Pothuraju T et al (2014) Effect of operational parameters on heavy metal removal by electrocoagulation. Environ Sci Pollut Res 21:14166–14173. https://doi.org/10.1007/s11356-014-3331-8

Burakov AE, Galunin EV, Burakova IV et al (2018) Ecotoxicology and Environmental Safety Adsorption of heavy metals on conventional and nanostructured materials for wastewater treatment purposes : A review. Ecotoxicol Environ Saf 148:702–712. https://doi.org/10.1016/j.ecoenv.2017.11.034

Channa AM, Baytak S, Memon SQ, Talpur MY (2019) Equilibrium, kinetic and thermodynamic studies of removal of phenol from aqueous solution using surface engineered chemistry. Heliyon 5. https://doi.org/10.1016/j.heliyon.2019.e01852

Chen X, Hossain MF, Duan C et al (2022) Isotherm models for adsorption of heavy metals from water - A review. Chemosphere 307:135545. https://doi.org/10.1016/j.chemosphere.2022.135545

Di Natale F, Gargiulo V, Alfè M (2020) Adsorption of heavy metals on silica-supported hydrophilic carbonaceous nanoparticles (SHNPs). J Hazard Mater 393:122374. https://doi.org/10.1016/j.jhazmat.2020.122374

Elabbas S, Adjeroud N, Mandi L et al (2020) Eggshell adsorption process coupled with electrocoagulation for improvement of chromium removal from tanning wastewater. Int J Environ Anal Chem 00:1–13. https://doi.org/10.1080/03067319.2020.1761963

Eletta OAA, Ayandele FO, Adeniyi AG, Ighalo JO (2019) Valorisation of sunflower (Tithonia Diversifolia) stalk for the removal of Pb (II) And Fe (II) from aqueous solutions. In Proceedings of the 49th NSChE Annual Conference, pp 107–116.

Guan W, Tian S, Cao D et al (2017) Electrooxidation of nickel-ammonia complexes and simultaneous electrodeposition recovery of nickel from practical nickel-electroplating rinse wastewater. Electrochim Acta 246:1230–1236. https://doi.org/10.1016/j.electacta.2017.06.121

Hakizimana JN, Gourich B, Chafi M et al (2017) Electrocoagulation process in water treatment: A review of electrocoagulation modeling approaches. Desalination 404:1–21. https://doi.org/10.1016/j.desal.2016.10.011

Heidmann I, Calmano W (2008) Removal of Zn(II), Cu(II), Ni(II), Ag(I) and Cr(VI) present in aqueous solutions by aluminium electrocoagulation. J Hazard Mater 152:934–941. https://doi.org/10.1016/j.jhazmat.2007.07.068

Huang CH, Shen SY, Dong CD, Kumar M, Chang JH (2020) Removal mechanism and effective current of electrocoagulation for treating wastewater containing Ni (II), Cu (II), and Cr (VI). Water 12(9):2614. https://doi.org/10.3390/w12092614

Hubetska TS, Kobylinska NG, García JR (2021) Sunflower biomass power plant by-products: Properties and its potential for water purification of organic pollutants. J Anal Appl Pyrol 157. https://doi.org/10.1016/j.jaap.2021.105237

Ii CN, Ii C, Vi C (2020) Removal mechanism and e ff ective current of electrocoagulation for treating wastewater

Ika Pratiwi N, Mukimin A, Zen N, Septarina I (2021) Integration of electrocoagulation, adsorption and wetland technology for jewelry industry wastewater treatment. Sep Purif Technol 279:119690. https://doi.org/10.1016/j.seppur.2021.119690

Jain M, Garg VK, Garg UK et al (2015) Cadmium removal from wastewater using carbonaceous adsorbents prepared from sunflower waste. Int J Environ Res 9:1079–1088. https://doi.org/10.22059/ijer.2015.995

Jain M, Garg VK, Kadirvelu K, Sillanpää M (2016) Adsorption of heavy metals from multi-metal aqueous solution by sunflower plant biomass-based carbons. Int J Environ Sci Technol 13:493–500. https://doi.org/10.1007/s13762-015-0855-5

Jain M, Garg VK, Paliwal R et al (2020) Optimization of cadmium(II) removal from water using sunflower waste carbon–a statistical approach. Toxin Rev 0:1–10. https://doi.org/10.1080/15569543.2020.1718163

Jaishankar M, Tseten T, Anbalagan N et al (2014) Toxicity, mechanism and health effects of some heavy metals. Interdiscip Toxicol 7:60–72. https://doi.org/10.2478/intox-2014-0009

Jean Claude N, Shanshan L, Khan J et al (2022) Waste tea residue adsorption coupled with electrocoagulation for improvement of copper and nickel ions removal from simulated wastewater. Sci Rep 12:1–18. https://doi.org/10.1038/s41598-022-07475-y

Jiang Y, Pang H, Liao B (2009) Removal of copper(II) ions from aqueous solution by modified bagasse. J Hazard Mater 164:1–9. https://doi.org/10.1016/j.jhazmat.2008.07.107

Jiang D, Yang Y, Huang C et al (2019) Removal of the heavy metal ion nickel (II) via an adsorption method using flower globular magnesium hydroxide. J Hazard Mater 373:131–140. https://doi.org/10.1016/j.jhazmat.2019.01.096

Kane SN, Mishra A, Dutta AK (2016) Preface: International Conference on Recent Trends in Physics (ICRTP 2016). J Phys: Conf Ser 755. https://doi.org/10.1088/1742-6596/755/1/011001

Khan MU, Malik RN, Muhammad S (2013) Human health risk from Heavy metal via food crops consumption with wastewater irrigation practices in Pakistan. Chemosphere 93:2230–2238. https://doi.org/10.1016/j.chemosphere.2013.07.067

Khan J, Lin S, Nizeyimana JC et al (2021) Removal of copper ions from wastewater via adsorption on modified hematite (α -Fe 2 O 3) iron oxide coated sand. J Clean Prod 319:128687. https://doi.org/10.1016/j.jclepro.2021.128687

Kong M, Wang L, Chao J et al (2019) Removal of Cu2+ and Ni2+ from Wastewater by using modified alkali-leaching residual wire sludge as low-cost adsorbent. Water, Air Soil Pollut 230. https://doi.org/10.1007/s11270-018-4071-z

Kumari S, Khan AA, Chowdhury A et al (2020) Efficient and highly selective adsorption of cationic dyes and removal of ciprofloxacin antibiotic by surface modified nickel sulfide nanomaterials: Kinetics, isotherm and adsorption mechanism. Colloids Surf, A 586:124264. https://doi.org/10.1016/j.colsurfa.2019.124264

Lekhlif B, Oudrhiri L, Zidane F et al (2014) Study of the electrocoagulation of electroplating industry wastewaters charged by nickel (II) and chromium (VI). J Mater Environ Sci 5:111–120

Liakos EV, Mone M, Lambropoulou DA et al (2021) Adsorption evaluation for the removal of nickel, mercury, and barium ions from single-component and mixtures of aqueous solutions by using an optimized biobased chitosan derivative. Polymers 13:1–20. https://doi.org/10.3390/polym13020232

Lu C, Liu C, Rao GP (2008) Comparisons of sorbent cost for the removal of Ni2+ from aqueous solution by carbon nanotubes and granular activated carbon. J Hazard Mater 151:239–246. https://doi.org/10.1016/j.jhazmat.2007.05.078

Matouq M, Jildeh N, Qtaishat M et al (2015) The adsorption kinetics and modeling for heavy metals removal from wastewater by Moringa pods. J Environ Chem Eng 3:775–784. https://doi.org/10.1016/j.jece.2015.03.027

Mohamed MA, Jaafar J, Ismail AF, Othman MHD, Rahman MA (2017) Fourier transform infrared (FTIR) spectroscopy. Membrane characterization, pp 3–29. https://doi.org/10.1016/B978-0-444-63776-5.00001-2

Mohammed AA (2015) Biosorption of lead, cadmium, and zinc onto sunflower shell : equilibrium, kinetic, and thermodynamic. Studies 16:91–105

Mousavi SH, Samakchi S, Kianfar M et al (2023) Raw sunflower seed shell particles as a green adsorbent for the adsorption of synthetic organic dyes from wastewater. Environ Prog Sustainable Energy 42:1–14. https://doi.org/10.1002/ep.14017

Oden MK (2020) Treatment of CNC industry wastewater by electrocoagulation technology: an application through response surface methodology. Int J Environ Anal Chem 100:1–19. https://doi.org/10.1080/03067319.2019.1628955

Om Prakash M, Gujjala R, Panchal M, Ojha S (2020) Mechanical characterization of arhar biomass based porous nano activated carbon polymer composites. Polym Compos 41:3113–3123. https://doi.org/10.1002/pc.25602

Patil CS, Gunjal DB, Naik VM et al (2019) Waste tea residue as a low cost adsorbent for removal of hydralazine hydrochloride pharmaceutical pollutant from aqueous media: An environmental remediation. J Clean Prod 206:407–418. https://doi.org/10.1016/j.jclepro.2018.09.140

Rathour R, Das P, Aikat K (2016) Microwave-assisted synthesis of graphene and its application for adsorptive removal of malachite green: thermodynamics, kinetics and isotherm study. Desalin Water Treat 57:7312–7321. https://doi.org/10.1080/19443994.2015.1020507

Sahu O, Mazumdar B, Chaudhari PK (2014) Treatment of wastewater by electrocoagulation: A review. Environ Sci Pollut Res 21:2397–2413. https://doi.org/10.1007/s11356-013-2208-6

Salem MA, Majeed N (2019) Removal of Cadmium from Industrial Wastewater using Electrocoagulation Process. J Eng 26:24–34. https://doi.org/10.31026/j.eng.2020.01.03

Sano Y, Bai X, Amagai S, Nakayama A (2018) Effect of a porous spacer on the limiting current density in an electro-dialysis desalination. Desalination 444:151–161. https://doi.org/10.1016/j.desal.2018.01.034

Shaker OA, Matta ME, Safwat SM (2021) Nickel and chromium removal by electrocoagulation using copper electrodes. Desalin Water Treat 213:371–380. https://doi.org/10.5004/dwt.2021.26722

Shaker OA, Safwat SM, Matta ME (2023) Nickel removal from wastewater using electrocoagulation process with zinc electrodes under various operating conditions: performance investigation, mechanism exploration, and cost analysis. Environ Sci Pollut Res 30:26650–26662. https://doi.org/10.1007/s11356-022-24101-6

Sikdar D, Goswami S, Das P (2020) Activated carbonaceous materials from tea waste and its removal capacity of indigo carmine present in solution: synthesis, batch and optimization study. Sustain Environ Res 30. https://doi.org/10.1186/s42834-020-00070-8

Spanos I, Auer AA, Neugebauer S et al (2017) Standardized benchmarking of water splitting catalysts in a combined electrochemical flow cell/inductively coupled plasma-optical emission spectrometry (ICP-OES) Setup. ACS Catal 7:3768–3778. https://doi.org/10.1021/acscatal.7b00632

Šuránek M, Melichová Z, Kureková V et al (2021) Removal of nickel from aqueous solutions by natural bentonites from slovakia. Materials 14:1–14. https://doi.org/10.3390/ma14020282

Tadayon Y, Bahrololoom ME, Javadpour S (2023) An experimental study of sunflower seed husk and zeolite as adsorbents of Ni(II) ion from industrial wastewater. Water Resour Indust 30:100214. https://doi.org/10.1016/j.wri.2023.100214

Tanong K, Tran LH, Mercier G, Blais JF (2017) Recovery of Zn (II), Mn (II), Cd (II) and Ni (II) from the unsorted spent batteries using solvent extraction, electrodeposition and precipitation methods. J Clean Prod 148:233–244. https://doi.org/10.1016/j.jclepro.2017.01.158

Taylor P, Jain M, Garg VK, Kadirvelu K (n.d.) Desalination and Water Treatment Removal of Ni (II) from aqueous system by chemically modified sunflower biomass 37–41. https://doi.org/10.1080/19443994.2013.811112

Vasudevan S, Lakshmi J, Sozhan G (2011) Effects of alternating and direct current in electrocoagulation process on the removal of cadmium from water. J Hazard Mater 192:26–34. https://doi.org/10.1016/j.jhazmat.2011.04.081

Wagle D, Lin CJ, Nawaz T, Shipley HJ (2020) Evaluation and optimization of electrocoagulation for treating Kraft paper mill wastewater. J Environ Chem Eng 8:103595. https://doi.org/10.1016/j.jece.2019.103595

Yan P, Mensah J, Adesina A et al (2020) Highly-dispersed Ni on BEA catalyst prepared by ion-exchange-deposition-precipitation for improved hydrodeoxygenation activity. Appl Catal B 267:118690. https://doi.org/10.1016/j.apcatb.2020.118690

Yargiç AS, Yarbay Şahin RZ, Özbay N, Önal E (2015) Assessment of toxic copper(II) biosorption from aqueous solution by chemically-treated tomato waste. J Clean Prod 88:152–159. https://doi.org/10.1016/j.jclepro.2014.05.087

Yuan D, Zhao J, Zhang Q et al (2022) Highly efficient extraction of uranium from aqueous solution using imidazole functionalized core-shell sunflower-like superparamagnetic polymer microspheres: understanding adsorption and binding mechanisms. Journal of Materials Chemistry A 10:12656–12668. https://doi.org/10.1039/d2ta02669d

Zhang C, Wu BH, Ma MQ et al (2019) Ultrathin metal/covalent-organic framework membranes towards ultimate separation. Chem Soc Rev 48:3811–3841. https://doi.org/10.1039/c9cs00322c

Authors and Affiliations

Jean Claude Nizeyimana[1,2,3] · Pamphile Ndagijimana[4] · Junaid Khan[1] · Liu Xiangru[1] · Gratien Twagirayezu[3,5] · Habasi Patrick Manzi[2,3] · Olivier Irumva[6] · Chang-Ping Yu[2] · Anyi Hu[2] · Shanshan Lin[1]

✉ Shanshan Lin
linss071@nenu.edu.cn

Jean Claude Nizeyimana
nizeyeclaude570@gmail.com

Pamphile Ndagijimana
ndapamphile450@gmail.com

Junaid Khan
zhundh436@nenu.edu.cn

Liu Xiangru
liuxr881@nenu.edu.cn

Gratien Twagirayezu
tgratien0@gmail.com

Habasi Patrick Manzi
manzi@iue.ac.cn

Olivier Irumva
irolinho@gmail.com

Chang-Ping Yu
cpyuntu@ntu.edu.tw

Anyi Hu
ayhu@iue.ac.cn

[1] School of Environment Northeast, Normal University, Changchun 130117, China

[2] CAS Key Laboratory of Urban Pollutant Conversion of Urban Environment, Institute of Urban Environment, Chinese Academy of Sciences, Xiamen 136102, China

[3] University of Chinese Academy of Sciences, Beijing 100049, China

[4] School of Civil Engineering, Guangzhou University, Guangzhou 510006, China

[5] State Key Laboratory of Environmental Geochemistry, Institute of Geochemistry, Chinese Academy of Sciences, Guiyang 550002, Guizhou, China

[6] School of Science and Engineering, Tongji University, Shanghai 200092, China